Research Article Vol. 30, No. 23 / 7 Nov 2022 / Optics Express 42749
Optics EXPRESS

Design, fabrication, and characterization of a tunable LED-based illuminator using refractive freeform arrays

SHOHREH SHADALOU,[1] DUSTIN GURGANUS,[2] WILLIAM J. CASSARLY,[3] MATTHEW A. DAVIES,[2] AND THOMAS J. SULESKI[1,*]

[1]Dept. of Physics & Optical Science, University of North Carolina at Charlotte, Charlotte, NC 28223, USA
[2]Dept. of Mechanical Engineering and Engineering Science, University of North Carolina at Charlotte, Charlotte, NC 28223, USA
[3]Synopsys Inc., 1100 Hunt Club Drive, Wooster, OH 44691, USA
[*]tsuleski@uncc.edu

Abstract: Dynamic illumination using tunable freeform arrays can enable spatial light distributions of variable size with high uniformity from non-uniform sources through relatively small opposing lateral shifts applied to the freeform components. We present the design, manufacturing, and characterization of a tunable LED-based illuminator using custom freeform Alvarez arrays with commercially available optics to shorten the manufacturing cycle. The optomechanical design and manufacturing of the Alvarez lens arrays and mounting parts are presented in detail. The optical performance of the system is evaluated and compared with simulation results using a custom camera-based test station. Experimental results demonstrate and confirm the dynamic illumination concept with good uniformity.

1. Introduction

Most illumination systems assume static relationships between the input source and the output illuminance pattern. Continuously variable illumination patterns can be advantageous in a range of applications including, for example modern lighting, automotive, medicine, dermatology, and lithography. Output patterns with good uniformity are preferable to eliminate lighting faults that degrade system performance or visual perception [1]. Energy savings is also an important factor in the design of illumination systems, with light-emitting diode (LED) sources used to improve efficiency. In addition to low power consumption, LEDs are more reliable, controllable, with longer life compared with traditional lighting sources [2].

Dynamic spatial light distribution for lighting application have been previously achieved by changing spacing between elements along the optical axis, which can result in undesirable pattern non-uniformity [3,4]. Lens arrays may be used to help enhance homogeneity of the system, but the longitudinal shift may still be undesirable in some compact systems [5,6]. Liquid lenses can also provide adjustable optical power with high tuning range [7–9]. However, such elements can results in disadvantages such as temperature and gravity sensitivities, sealing, and evaporation challenges [10]. Soft solid elastomer lenses can also provide tunable optical power but with a very limited tuning range due to high material stiffness [11,12].

Advances in design, manufacturing, and precision metrology have enabled use of freeform optics in advanced system designs [13,14]. As one example, freeform elements can enable tunability through the use of Alvarez lenses, which generate variable spherical power through relative lateral translation between a pair of plano-cubic elements in opposing directions [15]. However, coupling a single Alvarez lens to the non-uniform LED source does not improve uniformity. We previously reported the use of arrays of Alvarez lenses to address this issue for a tunable illumination system that enables continuous variable illumination from spot mode to

#474842 https://doi.org/10.1364/OE.474842
Journal © 2022 Received 2 Sep 2022; revised 18 Oct 2022; accepted 20 Oct 2022; published 4 Nov 2022

Optics EXPRESS

uniform flood mode, as shown in Fig. 1 [16]. The use of arrays enhances the uniformity of the target illuminance pattern, while the lateral (rather than longitudinal) shifts between components reduce the system package size. This approach enables the desired performance, but requires multiple custom components, which makes fabrication more difficult and time-consuming.

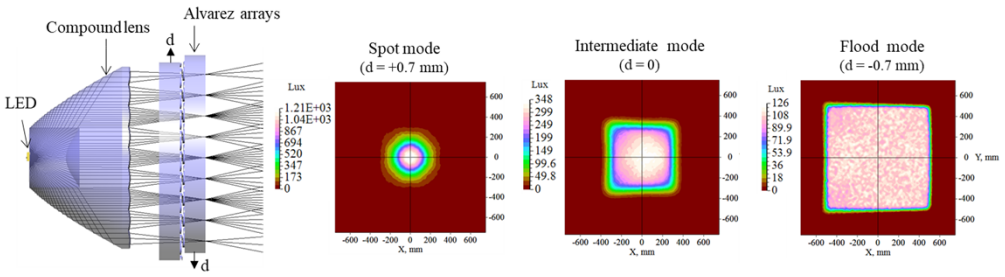

Fig. 1. The illuminance patterns of a dynamic illuminator at three selected modes at 2 m distance, from Ref. [16].

In this paper, we adapt our previous design approach to realize a dynamic illumination system with high uniformity by combining a Lambertian LED source with commercial-off-the-shelf (COTS) optics and custom arrays of Alvarez lenses. Using the COTS elements in the design speeds up the process of building a demonstrator. Section 2 reviews the implementation and simulation results of the refined optical design, and Section 3 presents the optomechanical design and required manufacturing processes. Section 4 reviews the implementation of a camera-based test station to measure the illuminance of the demonstrator, along with test results and analysis of optical performance, followed by conclusions in Section 5.

2. Design realization

We previously reported on a design approach for dynamic illumination systems enabling continuous variable illumination from spot mode to uniform flood mode, as shown in Fig. 1 [16]. This illuminator consists of a Lambertian LED source, a custom compound lens including a total-internal-reflection (TIR) lens for collimating the light, a lens array for distributing the light into convergent ray bundles, and Alvarez arrays for dynamically adjusting the size of the illumination pattern. In this section, this approach is adopted for a refined illumination system that utilizes COTS elements.

A COTS compound LED lens (KHATOD, PL1672) that combines a TIR lens with an integrated lens array and generates a full angle ~ 12° by 18° at half max replaces the custom compound TIR lens in the original design [16]. This COTS compound lens was paired with a matching LED module (Centaurus Cree LED module by LUXdrive), which eliminates the soldering process of attaching the LED to the PC board and eases alignment challenges. The 'static' section of the design is constructed by attaching the compound lens to the LED module, as shown in Fig. 2. This static portion must be modeled before it can be used as a module in the dynamic illumination design. The default LightTools source library was used to retrieve the optical model of this domed LED source (flux = 100 lumens, LED chip size 1.5 mm-by-1.5 mm). The size and radius of curvature (ROC) of each lenslet in the array are critical design parameters. The size of each lenslet was reported as 4 mm by 6 mm in the datasheet, but the optical form of the lenslets was not available from the vendor. As a consequence, an inverse engineering process was necessary, as described in [17]. The ROC was measured as 10.45 ± 0.1 mm using scanning white-light interferometry.

The 'dynamic' section of the system, consisting of the transmissive Alvarez arrays, was also modeled in LightTools with same unit size as the static lens array (4 mm-by-6 mm). The

Optics EXPRESS

Fig. 2. Constructing the static part of the tunable illuminator using the COTS optics.

system was initiated and simultaneously optimized over spot and flood illumination modes. The collimated merit function was set for spot mode and a uniform rectangular-shape target merit function with an average Full-Width Half Max ($FWHM_{Avg}$) of 1000 mm at 2 m from the source was set for the flood mode. The lenslet aperture shape defines the shape of the output light distribution, so the width-to-length ratio of the target pattern was set to the same value as the lenslets. The air gap between the Alvarez arrays was set at 0.5 mm. Additional polynomial terms were added to the basic Alvarez surface equations to minimize distortion defects in flood mode, as presented in [17]. The resulting surface equation for each element in the Alvarez array is given by:

$$z = 0.05\left(\frac{x^3}{3} + xy^2\right) + 0.019x^2 + 0.0241y^2 - 0.006x^2y^2 - 0.18x. \tag{1}$$

The final geometry of the dynamic illumination system is illustrated in Fig. 3. Simulated illuminance patterns (with 1,000,000 traced rays) for three chosen modes within the continuous variable illumination range are shown in Fig. 4. The transfer efficiency, defined as the incident flux over the target plane to the total emitted flux from the LED source, is ~75% including Fresnel losses and ~96% in the absence of Fresnel losses, indicating a highly efficient design.

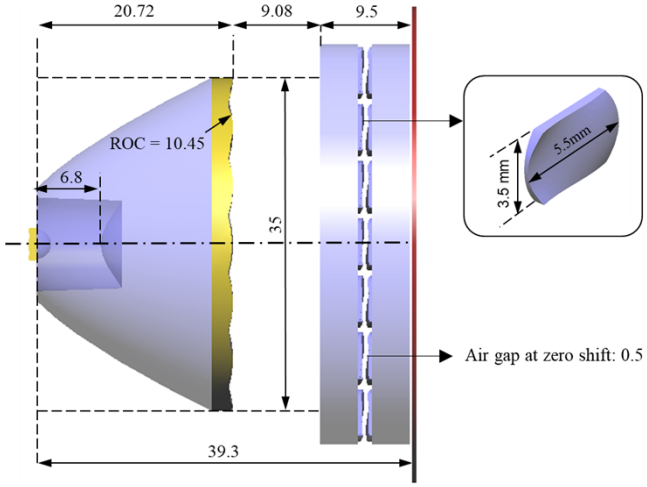

Fig. 3. The final geometry of the tunable LED-based illuminator (all units in mm).

Optics EXPRESS

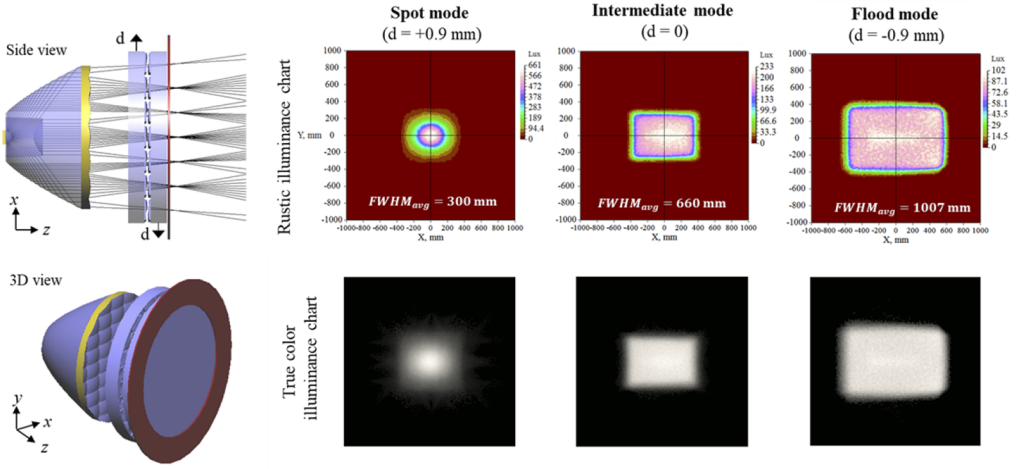

Fig. 4. Simulated illuminance patterns for spot, intermediate, and flood modes at 2 m from the source.

3. Optical and optomechanical fabrication

3.1. Optical system architecture

As discussed above, variable focal length of the Alvarez lenslet arrays is achieved by lateral relative translational movement between the freeform elements. While fully translational sets of optics are the intended use case, the optomechanical system would utilize precision machined flexures or translational mounts, which can be time and resource intensive for sourcing or manufacturing. To expedite manufacturing and allow for more stable alignment and testing, we chose instead to manufacture three sets of Alvarez arrays with pre-set physical shifts (Fig. 5) in the surfaces corresponding to the desired illumination modes shown in Fig. 4.

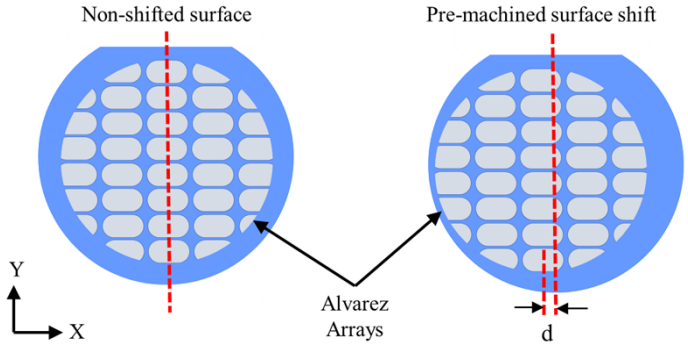

Fig. 5. Simplified image of shifted and unshifted Alvarez array surfaces.

The resulting optical system architecture, shown in Fig. 6, consists of one rear mounting plate, one optical barrel, the LED source, the COTS TIR lens, two steel alignment pins, four magnets (two for each mount), and the custom Alvarez arrays.

3.2. Manufacturing of optomechanical fixturing

The main goals for the optomechanical design were controlling spatial tolerances, reducing part count, and testing system compatibility. To these ends, the system was designed with a main

Optics EXPRESS

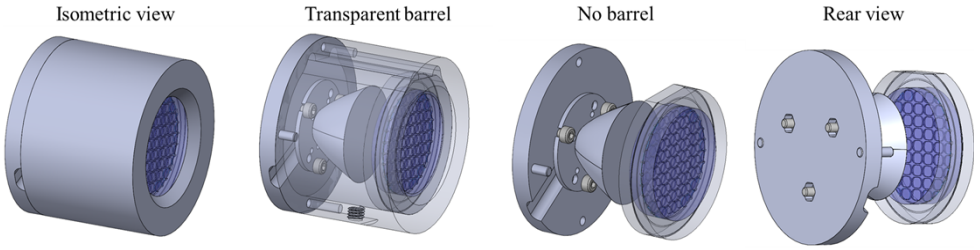

Fig. 6. Multiple views of CAD model for Alvarez array illumination system.

housing consisting of one back mounting plate and an optical barrel to set the distances between the components. The plate and barrel were all machined from the same piece of aluminum (6061) bar stock with 63.5 mm outer diameter to facilitate tolerance and alignment preservation. The plate and barrel were each machined on the HAAS Computer Numerically Controlled (CNC) Toolroom mill (Fig. 7).

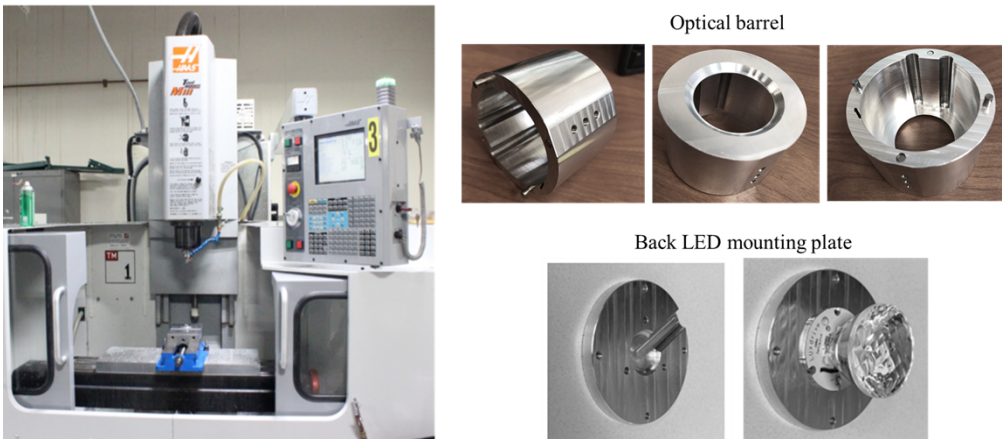

Fig. 7. A HAAS CNC Toolroom Mill at UNC Charlotte with manufactured mountings.

One issue with the initial manufacturing of this mounting system was machining the center of the optical barrel. The overall length of the mounting is 51 mm, with the optical barrel bore at 41 mm deep. This bore depth can lead to manufacturing problems like tool chatter and undercutting caused by tool deflection. To limit these issues the diameter of the milling tool was increased to 19.05 mm and tool shank relieved so it could reach full depth of cut without colliding with the barrel. A thin plastic spacer was designed and 3D printed to hold the optics in place in the optical barrel. Hardened steel machine pins with outer diameters of 3.175 mm and neodymium magnets were used to clock and hold the housings together for testing. Magnets were selected instead of fasteners (such as threaded rods or bolts) to avoid an over-constrained system. The magnets also simplify changing the Alvarez array components for the different illumination modes.

3.3. Optical Fabrication

Freeform surface manufacturing requires at least three axes of motion [14,18–21]. The Alvarez arrays in our system were fabricated with a multi-axis ultraprecision diamond milling center with a 50,000 RPM milling spindle. Direct milling of the freeform surfaces was done using a diamond mill on three axes (X, Y, Z). While less common than a diamond turning of optical

Optics EXPRESS

surfaces, diamond milling can enable the generation of optical surfaces with steeper slopes than are achievable with diamond turning [22–25].

The freeform arrays were machined in two separate processes: (1) preparation of the optical blanks, and (2) ultraprecision diamond milling of the freeform optical surfaces. Initial blanking began with rough cutting of 50.8 mm diameter PMMA bar stock on a horizontal band saw into approximately 5 mm thick disks. These disks were then faced with a diamond tool with 1.008 mm tool nose radius on the Moore Nanotech 350FG using a 38.1 mm diameter aluminum vacuum chuck. The Moore Nanotech 350FG (Fig. 8), is a 5-axis precision diamond machining center with 3 linear axes (X, Y, Z) with 0.034 nm resolution and two rotary axes (B, C) with 1.75 nanoradian resolution. Total manufacturing volume on this machine is 350 mm by 150 mm by 300 mm (X, Y, Z). The machine is enclosed in a temperature-controlled room at 20 C +/- 0.1 degrees C at 50% relative humidity to minimize thermal variations during manufacturing.

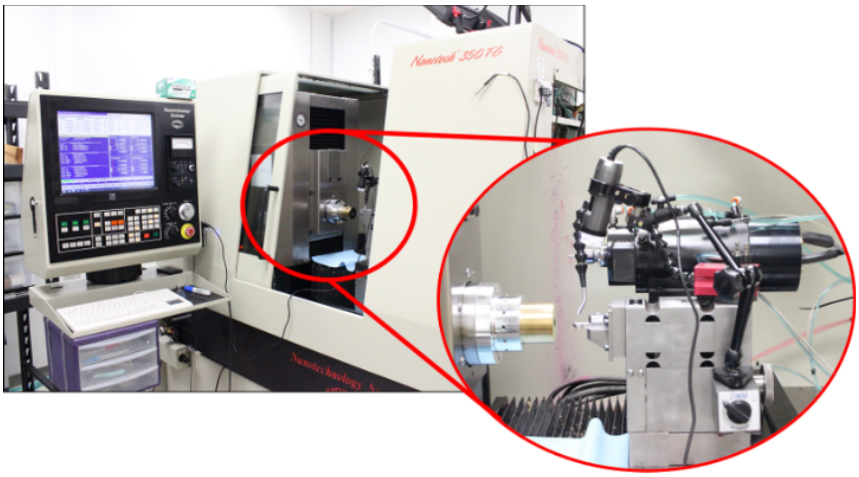

Fig. 8. Moore Nanotech 350FG 5-axis ultraprecision diamond machining system at UNC Charlotte.

Once the rough-cut blanks have been faced on the front and back sides, the parts were milled on a HAAS Toolroom Mill using a jig to cut clocking flats for angular alignment of the parts. The outer diameters of the steel machine pins aligned with a circumscribed circle which matched with the optic's outer diameter. This design enables an endmill with a known diameter to cut a flat on the outer diameter of the optical blank.

After the clocking flats were machined, the optical blanks were taken back to the Moore Nanotech 350FG for final freeform machining. Both faces of all optical blanks were diamond turned to ±1 µm parallelism and the desired starting thickness. Three sets of Alvarez arrays, each set with the same form with the prescribed global surface shift, were then manufactured from the optical blanks using diamond milling on the Moore Nanotech 350FG (Fig. 9).

Complex freeform toolpaths were generated using NanoCAM4, a precision manufacturing software package which allows for the direct import of the surface equations and tooling parameters. The toolpaths were built by first importing the surface equation for a single Alvarez lenslet (Eq. (1) above) into NanoCAM4. This singular lenslet surface was exported as a point cloud and compared to a MATLAB generated interpolant map from the same prescription. This comparison showed no error between the two separately generated maps, validating that the optical surface in NanoCAM4 was correct. The validated lenslet surface in NanoCAM4 was then duplicated in the software to form an array. From that point, the milling tool was defined in the software and the toolpath was post-processed. The optical data within NanoCAM4 were offset

Optics EXPRESS

by the required distances along the x-axis for each Alvarez array (−900, 0, or +900 µm, as shown in Figs. 4 and 5) and then the toolpaths were processed and exported for usage on the Moore Nanotech 350FG.

The optics were mounted for final surface cutting used a 10 PSI vacuum and a layout fluid. Layout fluid is a thin liquid, useful for mounting small parts on a vacuum chuck. When it dries, the layout fluid can act as a thin adhesive with no adverse effects on PMMA, unlike some other glues. The optical blanks were clocked on the pre-milled flat to within ±1 µm. A diamond milling tool with a tool nose radius of 247 µm was used. Direct milling of the surface began with roughing passes at a 50 µm depth of cut with 50 mm/min feedrate, and 5µm data density. A single finish pass was performed at a 10 µm depth of cut, 10 mm/min feed rate, and 0.5 µm data density. The resulting plastic freeform elements are conducive to molding for larger quantities.

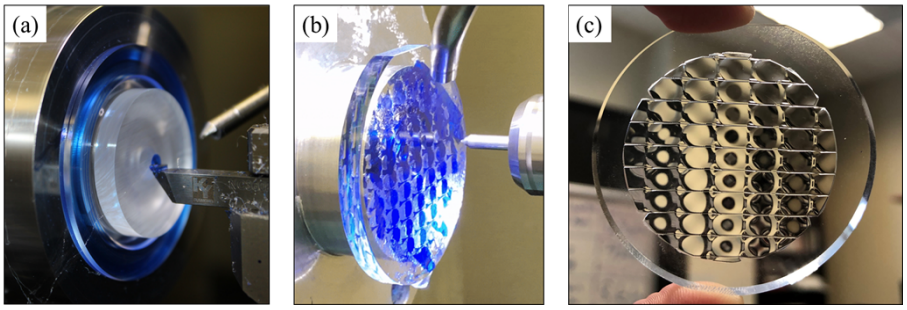

Fig. 9. (a) Diamond turning of surface flat, (b) Diamond milling of the optical surface, (c) Example of final optic.

We were unable to measure the form of the resulting freeform optics at this time, but from prior experience we expect the form accuracy on the Moore Nanotech 350FG to be better than 0.25 µm Peak-to-Valley (PV) [26]. Surface finish was measured using the Zygo Zegage Plus 3D optical surface profiler (Fig. 10) on two separate Alvarez array plates. The optical surfaces were measured using 20x and 50x objectives with 3 averages and a Gaussian bandpass filter of 2.5 to 80 µm, following ISO 10110-8 [27]. These filters were chosen to isolate surface roughness from form and waviness. The average surface roughness (Sa) from measurements across the phase plate surfaces was 25 nm.

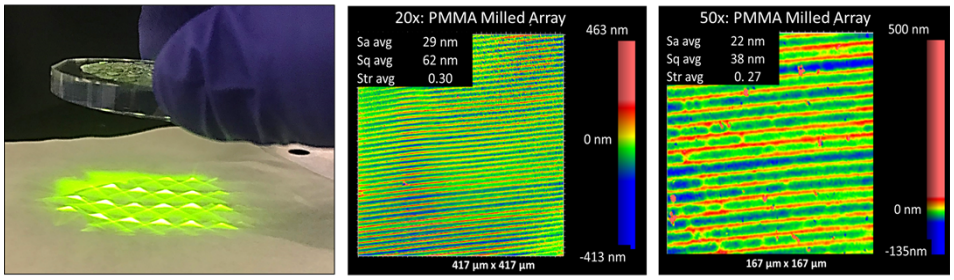

Fig. 10. Measurement of a finished Alvarez lenslet array and the average surface roughness measurements.

Optics EXPRESS

4. Performance characterization methods and results

4.1. Test system development and calibration

Optical performance analysis of an illumination system may be conducted using a variety of photometric quantities, including illuminance, intensity, and luminance. Illuminance is a good option for luminaires which defines the amount of luminous flux per unit area on a target plane (lumen/m^2, or lux) [28].

Measurement of illuminance values at selected test points over the target plane provides a general method for defining uniformity of the illuminance pattern, with the grid size used to cover the test area varying according to different test standards [29]. This simple approach comes with potential disadvantage of missing information since the measurements are taken at discrete points on the target plane. The measurement process also can be time consuming if a luxmeter is used to measure the illuminance over the test points one-by-one. Another approach to characterize the illuminance pattern is capturing the light distribution projected on a diffused screen which provides a better understanding of the light distribution. However, commercially available calibrated test setups can be very costly. To address these issues, we developed a low-cost calibrated camera-based test station to characterize the illuminance pattern across a target plane. This test station includes a CMOS camera (FLIR BFS-U3-13y3M-C) with a 6 mm fixed-focal-length lens mounted on top of the dynamic illuminator. The monochromatic camera captured the light pattern projected on a semi-Lambertian MaxWhite® diffusing screen [30] set at 2 m distance, as shown in Fig. 11.

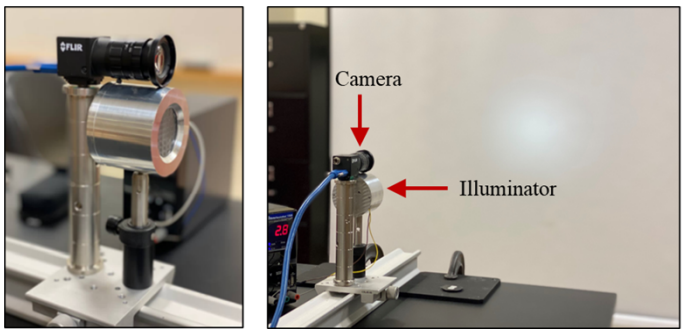

Fig. 11. Custom camera-based test station for illuminance measurement.

A voltage stabilizer was connected to the LED source of the illuminator to regulate the input power. The test experiments were performed at 700 mA operating current with 3V running voltage at room temperature. The LED was run for ~24 hours before testing to reduce initial ageing effects. The body of the assembly in contact with the LED served as a nominal heat sink. The test station was calibrated for both distortion and illuminance as described below.

Distortion calibration was performed by estimating the geometrical parameters of the camera using the "Camera Calibrator" app in MATLAB [31]. As inputs, 20 different images of a standard checkerboard were captured by the CMOS camera at different locations and orientations. We used an adjustable monitor as a holder for positioning a printed checkerboard test sheet at different rotation and tilt angles. An image of the checkerboard before and after correction for camera lens distortion is shown in Fig. 12.

In next step, the illuminance was calibrated by comparing camera data with luxmeter data measured at selected test points in the light pattern generated from the static section of the illuminator (the LED and the compound TIR lens). First, as shown in Fig. 13, a pattern with a grid of points on 10 cm spacing was attached to the screen and an image of it was recorded as a reference. Then, the illuminance values at the test points were measured with an LED light meter

Optics EXPRESS

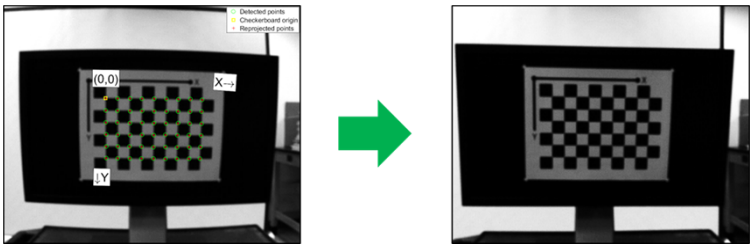

Fig. 12. Correcting camera lens distortion using the "Camera Calibrator" toolbox in MATLAB.

(LT45 EXTECH). The grid pattern was detached from the screen and multiple images of the light pattern were recorded with different camera gains and exposure times.

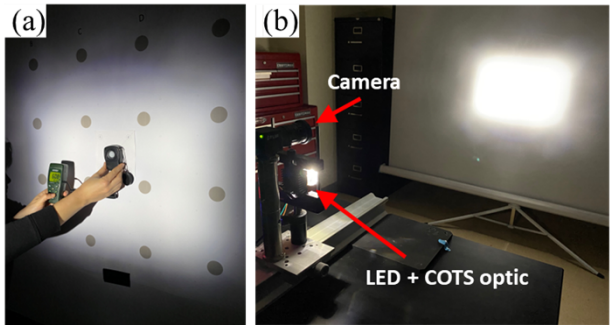

Fig. 13. Illuminance calibration process: (a) illuminance measurement by lux-meter, (b) capturing the light distribution by camera.

A custom code was developed in MATLAB to first correct for camera distortion as discussed above, and then crop the image to the desired size. The test point coordinates on the screen were then detected using image processing technique as shown in Fig. 14(a). The gray levels of the test points were extracted from the test images along with their coordinates. Linear regressions were performed to correlate the gray levels of the test points extracted from test images (between 0-255 for the 8-bit monochromatic camera) with the measured luxmeter data for the different camera settings. The camera setup with the minimum RMS error from the linear regressions was selected as the reference calibrated setup for subsequent measurements. The linear regression RMS error for the range of illuminance in this application (0 to ~ 650 lux) is acceptable. This process was performed to simplify obtaining the response curve of the camera. The detail of the chosen camera setup and the corresponding transfer function to correlate the image gray levels to the illuminance values are listed in Table 1. An illustration of the correlation between the camera image and luxmeter values for the chosen setup is shown in Fig. 14(b).

Table 1. Camera illuminance calibration and transfer function

Camera exposure time (mSec)	Camera gain	Illuminance transfer function (lux)	RMS error of linear regression (lux)
100	0.96	3.1965 (image grey level) + 7.04	6.78

4.2. Performance metrics and analysis software

We used two main performance metrics in this work to characterize the size and uniformity of

Optics EXPRESS

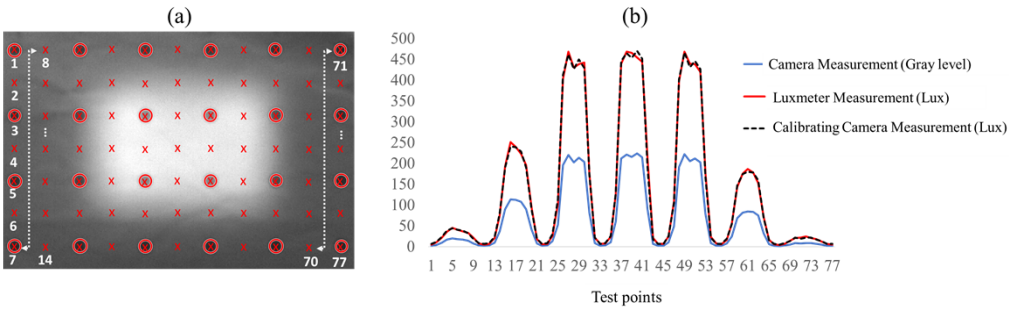

Fig. 14. (a) Detecting test points on the image to define locations by using MATLAB "imfindcircles", and (b) Correlating camera to luxmeter measurements using linear regression over test points.

the illuminance patterns: (1) The average full width at half of the maximum value of the light distribution ($FWHM_{Avg}$) which is equal to the diameter of the circle with the same area as the area limited by FWHM; and (2) the Average Deviation (AD) as a statistical representation of illumination uniformity, defined as:

$$AD = \frac{1}{E_{avg}}\sqrt{\frac{1}{N}\sum_{i=1}^{N}[E(i) - E_{avg}]^2}, \tag{2}$$

where E(i) is the illuminance value at each test point and E_{avg} is the illuminance average over all test points (N). We calculate AD over the area limited by $FWHM_{avg}$; zero AD corresponds to a perfectly uniform pattern.

MATLAB was used to create a standalone application to facilitate optical performance analysis. The graphical user interface (GUI) layout is shown in Fig. 15 for flood mode illumination as an example. The first column of the application connects to LightTools to upload simulation mesh results, and the user uploads the corresponding test image in the second column. Performance metrics to quantitatively characterize the illuminance patterns are then calculated automatically.

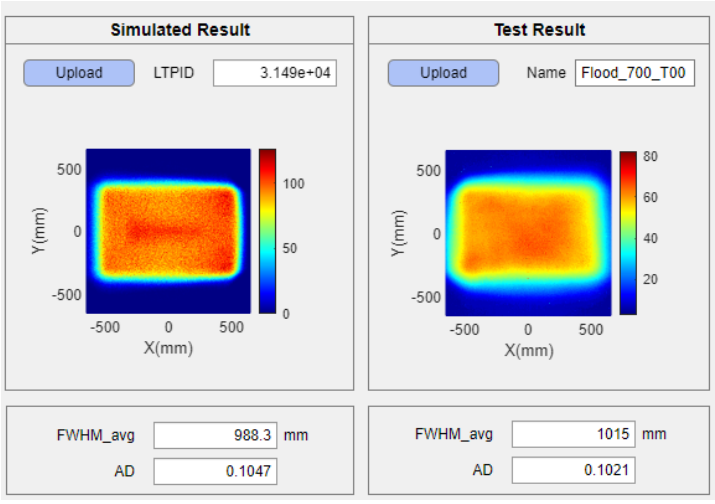

Fig. 15. Testing application to automate test post processing and compare the simulated and experimental results.

Optics EXPRESS

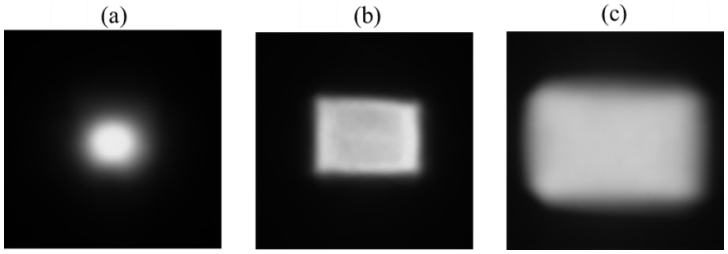

Fig. 16. Qualitative grayscale test images from the CMOS camera for the three selected illumination modes: (a) spot mode, (b) intermediate mode, and (c) flood mode.

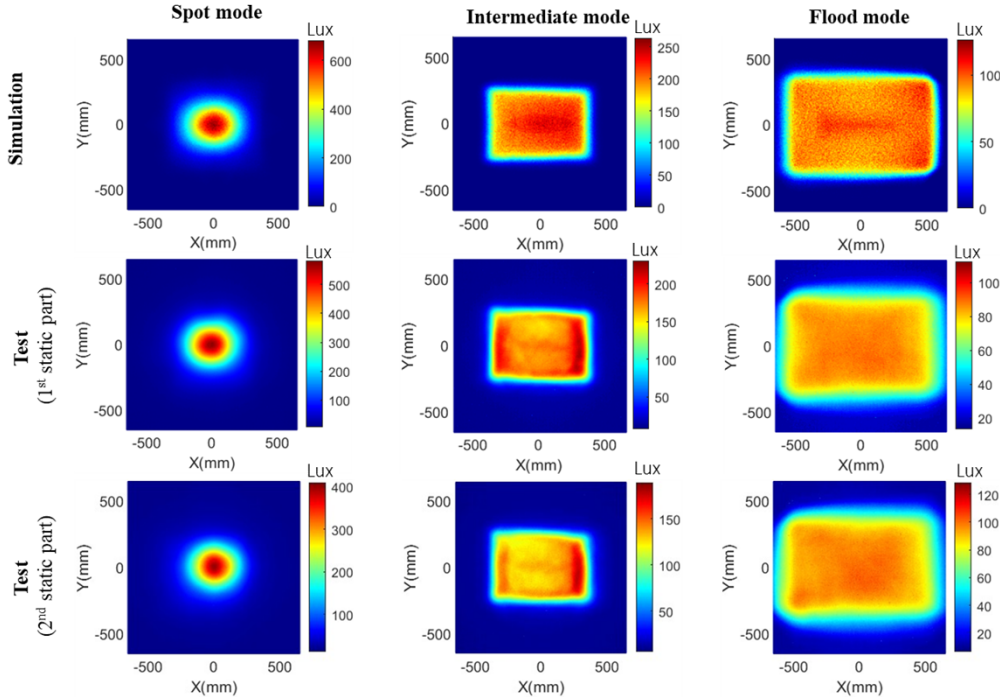

Fig. 17. Illuminance patterns of simulation and test results for three selected illumination mode from developed testing platform.

4.3. Testing results

The pairs of Alvarez arrays discussed in Section 3.1 were used to realize the spot, intermediate and flood modes. The testing process was repeated with two sets of static parts (LED + compound TIR lens) to provide limited qualitative data on variability from LED binning and optomechanical alignment. Qualitative test images are shown in Fig. 16. We note that the images in Fig. 16 were purposely overexposed to enable better visualization of the intermediate and flood modes. Quantitative measurements of each mode using the MATLAB tools discussed in Section 4.2 and camera settings of Table 1 are shown in Fig. 17.

These experimental results demonstrate the dynamic illumination concept with good uniformity. Small differences between simulated and test results can be seen in Fig. 17, which we believe result from surface scattering in the experimental parts and uncertainties in the simulations

Optics EXPRESS

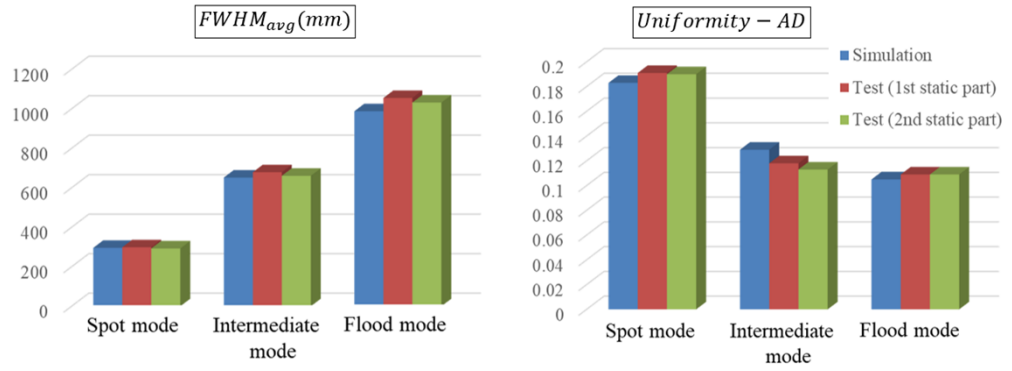

Fig. 18. Summary of performance metrics from simulated and experimental results.

due to the need to estimate some geometrical parameters for the COTS TIR lens. Additional comparisons of performance metrics for these results are shown in Fig. 18.

5. Conclusion

We have reported the design, manufacture, and characterization of a highly-efficient tunable LED-based illuminator. This system enables continuously variable light distributions with high uniformity from a non-uniform source through relatively small opposing lateral shifts applied to arrays of freeform Alvarez lenses. A commercially available TIR collimating optic was used in the demonstrator to reduce costs and manufacturing time. A stationary housing holding switchable freeform arrays was built as an alternative to a continuously shiftable mechanism to simplify the optomechanical design for proof of concept; mechanical or electrical actuators can be used to provide the necessary shiftable mechanism for future designs. Three sets of freeform arrays with pre-machined shifts corresponding to three selected modes of illumination were manufactured by Moore 350FG utilizing a diamond milling technique. A low-cost camera-based test station was developed and calibrated to characterize the output illuminance patterns across a target screen, and a user-friendly application was developed to evaluate optical performance including pattern size and uniformity.

Experimental results demonstrated and verified the dynamic illumination concept with good uniformity made possible by Alvarez arrays in an LED-based illuminator. Small discrepancies between the simulated and experimental results are attributed to uncertainty in geometrical parameters determined for the COTS TIR compound lens model. We note that the diamond milling manufacturing times for the freeform arrays are impractical for volume manufacturing, but that the resulting plastic freeform elements are conducive to molding for larger quantities.

Funding. National Science FoundationI/UCRC Center forr Freeform Optics (IIP-1822026, IIP-1822049).

Acknowledgments. The authors would like to thank Synopsys for providing the LightTools license and the Center for Precision Metrology at the University of North Carolina at Charlotte for collaboration on measuring the COTS TIR optics.

Disclosures. The authors declare no conflicts of interest.

Data availability. Data underlying the results presented in this paper are not publicly available at this time but may be obtained from the authors upon reasonable request.

Optics EXPRESS

References

1. A. J. Whang, S. Chao, C. Chen, Y. Chen, H. Hsiao, and X. Hu, "High uniform illumination of light-emitting diodes lighting with applying the multiple-curvature lens," Opt. Rev. **18**(2), 218–223 (2011).
2. J. M. Gee, J. Y. Tsao, and J. A. Simmons, "Prospects for LED lighting," Proc. SPIE **5187**, 227–233 (2004).
3. W. S. Lee, "Zoomable LED flashlight," U.S. Patent 9,068,727 B2 (30 Jun. 2015).
4. R. D. White and D.P. Weiss, "Lighting device with dynamic bulb position," U.S. Patent 4,339,788 (Jul. 13, 1982).
5. J. B. Lee, B. I. Chiang, and H. K. Ho, "Zoom spotlight using LED array," U.S. Patent 8,979,316 B2 (Mar. 17, 2015).
6. D. J. Stavely, U.S. Patent App. 2012/0121244 A1 (May 17, 2012).
7. M. Bueeler and M. Aschwanden, "Illumination source with variable divergence," U.S. Patent 8,944,647 B2 (Feb. 3, 2015).
8. D. Y. Zhang, V. Lien, Y. Berdichevsky, J. Choi, and Y. H. Lo, "Fluidic adaptive lens with high focal length tunability," Appl. Phys. Lett. **82**(19), 3171–3172 (2003).
9. N. T. Nguyen, "Micro-optofluidic Lenses: A review," Biomicrofluidics **4**(3), 031501 (2010).
10. Z. Yongchao, "Development of solid tunable optics for ultra-miniature imaging systems," Ph.D. dissertation (National University of Singapore, 2016).
11. G. Beadie, M. L. Sandrock, M. J. Wiggins, R. S. Shirk, M. Ponting, Y. Yang, T. Kazmierczak, A. Hiltner, and E. Baer, "Tunable polymer lens," Opt. Express **16**(16), 11847–11857 (2008).
12. P. Liebetraut, S. Petsch, W. Mönch, and H. Zappe, "Tunable solid-body elastomer lenses with electromagnetic actuation," Appl. Opt. **50**(19), 3268–3274 (2011).
13. E. Savio, L. D. Chiffre, and R. Schmitt, "Metrology of freeform shaped parts," CIRP Ann. **56**(2), 810–835 (2007).
14. J. P. Rolland, M. A. Davies, T. J. Suleski, C. Evans, A. Bauer, J. C. Lambropoulos, and K. Falaggis, "Freeform optics for imaging," Optica **8**(2), 161–176 (2021).
15. L. W. Alvarez and W. E. Humphrey, "Variable-power lens and system," U.S. Patent 3,507,565A (Apr. 21, 1970).
16. S. Shadalou, W. J. Cassarly, and T. J. Suleski, "Tunable illumination for LED-based systems using refractive freeform arrays," Opt. Express **29**(22), 35755–35764 (2021).
17. S. Shadalou, W. J. Cassarly, and T. J. Suleski, "Tunable LED-based illuminator using freeform arrays," Proc. SPIE **12078**, 17 (2021).
18. F. Z. Fang, X. D. Zhang, A. Weckenmann, G. X. Zhang, and C. Evans, "Manufacturing and measurement of freeform optics," CIRP Ann. **62**(2), 823–846 (2013).
19. M. A. Davies, C. J. Evans, R. R. Vohra, B. C. Bergner, and S. R. Patterson, "Application of precision diamond machining to the manufacture of microphotonics components," Proc. SPIE **5183**, 94–108 (2003).
20. K. Garrard, T. Bruegge, J. Hoffman, T. Dow, and A. Sohn, "Design tools for freeform optics," Proc. SPIE **5874**, 58740A (2005).
21. L. B. Kong and C. F. Cheung, "Design, fabrication and measurement of ultra-precision micro-structured freeform surfaces," CAIE **61**(1), 216–225 (2011).
22. B. McCall, G. Birch, M. Descour, and T. Tkaczyk, "Fabrication of plastic microlens arrays for array microscopy by diamond milling techniques," Opt. Eng **49**(10), 103401 (2010).
23. C. Huang, L. Li, and A. Y. Yi, "Design and fabrication of a micro Alvarez lens array with a variable focal length," Microsyst. Technol. **15**(4), 559–563 (2009).
24. E. Brinksmeier, R. Gläbe, and L. Schönemann, "Review on diamond-machining processes for the generation of functional surface structures," CIRP J. Manuf. Sci. and Technol. **5**(1), 1–7 (2012).
25. S. Scheiding, Y. Y. Allen, A. Gebhardt, R. Loose, L. Li, S. Risse, R. Eberhardt, and A. Tünnermann, "Diamond milling or turning for the fabrication of micro lens arrays: comparing different diamond machining technologies," Proc. SPIE **7927**, 79270N (2011).
26. . Moore Nanotechology Systems, in Nanotech 350FG Specification Overview, Swanzey, NH (2007).
27. International Organization for Standardization, "Optics and photonics - Preparation of drawings for optical elements and systems - ISO10110-8" (2010).
28. R. J. Koshel, *Illumination Engineering: design with nonimaging optics* (IEEE Press: John Wiley and Sons, 2013), Chap. 1.
29. D. J. Carter, R. C. Sexton, and M. S. Miller, "Field measurement of illuminance," LR&T **21**(1), 29–35 (1989).
30. Data sheet available at: https://elitescreens.com/wp-content/uploads/MaxWhite_MaterialSheet.pdf.
31. The MathWorks Inc. (R2020a), Camera Calibrator Toolboxhttps://www.mathworks.com/help/vision/ref/cameracalibrator-app.html.